A new method for quantitative XEDS tomography of complex heteronanostructures

Submitted to Particle & Particle Systems Characterization

A new method for quantitative XEDS tomography of complex hetero-nanostructures

*Daniele Zanaga, Thomas Altantzis, Lakshminarayana Polavarapu, Luis M. Liz-Marzán, Bert Freitag, Sara Bals**

D. Zanaga, Dr. T. Altantzis, Prof. Dr. S. Bals

EMAT, University of Antwerp, Groenenborgerlaan 171, B-2020 Antwerp, Belgium

Dr. L. Polavarapu, Prof. Dr. L.M. Liz-Marzán

Bionanoplasmonics Laboratory, CIC biomaGUNE, Paseo de Miramón 182, 20009 Donostia - San Sebastián, Spain

Dr. L. Polavarapu

Departamento de Química Física, Universidade de Vigo, 36310 Vigo, Spain

Prof. Dr. Luis M. Liz-Marzán

Ikerbasque, Basque Foundation for Science, 48013 Bilbao, Spain

Dr. B. Freitag

FEI Company, Building AAE, Achtseweg Noord 5, Eindhoven, The Netherlands

*** Corresponding author**

Submitted to Particle & Particle Systems Characterization

E-mail: sara.bals@uantwerpen.be

The authors declare no competing financial interest

Keywords: XEDS, quantification, electron tomography

Abstract

Reliable quantification of 3D results obtained by X-ray Energy Dispersive Spectroscopy (XEDS) tomography is currently hampered by the presence of shadowing effects and poor spatial resolution. Here, we present a method that overcomes these problems by synergistically combining quantified XEDS data and High Angle Annular Dark Field – Scanning Transmission Electron Microscopy (HAADF-STEM) tomography. As a proof of principle, the approach is applied to characterize a complex Au/Ag nanorattle obtained through a galvanic replacement reaction. However, the technique we propose here is widely applicable to a broad range of nanostructures.

1. Introduction

Over the last decades, electron tomography based on HAADF-STEM has evolved into a standard technique to investigate the morphology and inner structure of nanomaterials.[1] The HAADF-STEM intensity depends on sample thickness but also scales with the atomic number Z and therefore, chemical compositions can be studied from these three-dimensional (3D) reconstructions.[2, 3] Nevertheless, it is not straightforward to interpret the gray levels in a 3D HAADF-STEM reconstruction in an absolute manner. Therefore, it becomes very challenging to use HAADF-STEM tomography for samples in which mixing of elements is expected. Also for samples that contain unknown elements or elements with atomic number Z close to each other, HAADF-STEM tomography may no longer be informative.

However, it is well known that the properties and applications of nanostructures are strongly dependent on their morphology as well as their chemical composition.[4] Traditional electron microscopy techniques do not provide quantitative information on the composition of single nanoparticles. In an increasing number of recent studies, XEDS is combined with tomography to understand complex nanostructure morphology and composition in 3D. These studies rely on newly developed XEDS detectors[5, 6] such as the Super-X detection system, which consists of four individual detectors, symmetrically arranged around the TEM sample. Although qualitative results obtained by XEDS tomography have been reported,[7-10] it remains challenging to obtain quantitative information by 3D XEDS and therefore further progress is required. By using the Super-X detector, one is able to overcome problems that were previously related to extreme shadowing of the XEDS signal caused by the sample-detector configuration. Although this problem can be largely overcome, some shadowing effects remain,[11, 12] as illustrated in Figure 1. Since such shadowing effects vary for different tilt

angles, the XEDS signal integrated over the four detectors will also depend on the tilt angle[11-13] and the projection principle for electron tomography is no longer fulfilled.[12] Different methodologies have been proposed to overcome this challenge. For example, signals from individual detectors can be combined,[11, 14] the acquisition time can be adjusted as a function of the tilt angle[12] or the total signal for every map can be normalized to the same value.[13, 15] However, in order to maximize the signal-to-noise ratio, it is of great importance to collect as many counts as possible. Selectively switching off detectors is therefore disadvantageous, while changing the acquisition time improves the quality of the tilt series, but a calibration of the holder is required and the final result is still hampered by inaccuracies.[12] Normalizing the total signal for every map, works in minimizing the shadowing effect in the absence of absorption,[15] but the reconstructions obtained from the net counts maps still suffer from a poor spatial resolution, due to the noise and small number of projections.

Here, we propose an alternative approach to optimize the reconstruction of an XEDS tomography series by minimizing the impact of shadowing effects. The spatial resolution is furthermore improved through a combination with HAADF-STEM tomography. HAADF-STEM yields a relatively high signal-to-noise ratio, and does not suffer from shadowing effects other than those related to the "missing wedge".[1] XEDS, on the other hand, yields chemical information, even when no prior knowledge of the sample is available or for samples that contain elements with a small difference in atomic number Z. As a proof of principle, we apply our methodology to a nanostructure containing a mix of Au and Ag atoms. However, it must be noted that the approach we propose here enables quantitative 3D chemical characterization of a broad variety of nanostructures.

2. Methods

The current approach to obtain a quantitative 3D XEDS reconstruction is based on XEDS maps, from which the background is subtracted leading to net counts maps. These maps can be used directly as an input for a tomographic algorithm such that a different reconstruction for each element is obtained.[8, 9] Next, these reconstructions can be quantified by analyzing the voxel intensities using the Cliff-Lorimer or ζ-factor method.[14] The outcome of this approach is predominantly determined by the quality of the tomogram and therefore by the number of available projections. However, due to the relatively long acquisition times, XEDS tilt series are typically acquired with an increment that is larger in comparison to HAADF-STEM e.g. every 10º. Furthermore, noise and shadowing effects such as illustrated in Figure 1 will degrade the quality of the reconstruction. Shadowing effects affect the XEDS intensity and therefore, an XEDS map is not simply a function of sample thickness or chemical concentration. In this study, we overcome this problem by using maps based on the ratio between the X-ray intensity of one element over the sum of intensities of all elements. Such maps are not affected by shadowing effects since the XEDS counts for both types of elements are acquired at the same tilt angle and are influenced by shadowing in the same manner. This assumption is valid for "hard" X-rays with energies > 3 keV, else an absorption correction method[14, 16] should be applied.

A new approach to obtain ratio maps has been recently proposed, which is based on using the well-known ζ-factor method.[16] In short, the method is similar to the conventional Cliff-Lorimer method,[17] but presents major advantages regarding correction of absorption effects and experimental determination of the sensitivity factors, the so-called "ζ-factors". In this study, ζ-factors were determined from particles comprising a single element, through the technique described in a previous work[18] by combining XEDS analysis and electron tomography. Once the ζ-factors are known, quantification of XEDS data can be carried out.[16] By applying the ζ-factor method, reliable ratio maps are obtained, which are not

affected by shadowing effects. However, it is important to note that these maps no longer contain any information on sample thickness and consequently do not fulfill the projection requirement. Our approach therefore relies on combining these ratio maps with thickness information extracted from a HAADF-STEM reconstruction of the same nanostructure.

To measure the particle thickness, a HAADF-STEM reconstruction is computed using the SIRT algorithm.[19] The SIRT reconstruction is segmented to obtain a binary volume where voxel values are either equal to 1 if they belong to the particle or equal to 0 elsewhere. Next, the segmented STEM reconstruction is forward projected along the same directions as those that were used to acquire XEDS maps. The XEDS maps are then aligned to the forward projections using filtered normalized cross-correlation.[20] It should be noted that this approach does not require the XEDS and HAADF-STEM series to be acquired simultaneously or using the same experimental parameters. By multiplying the ratio maps with the relative particle thickness, extracted from 3D HAADF-STEM reconstructions, chemically quantified projections are obtained. The projections fulfill the projection requirement and contain reliable quantitative chemical information. These elemental projections are used as an input for a tomography algorithm and a quantified 3D reconstruction of the nanostructure is obtained, from which both the structure and the composition can be investigated. A schematic workflow of our approach is presented in Figure 2.

HAADF-STEM tomography yields a more accurate description of the particle shape and morphology, which can be used as prior knowledge in the reconstruction of the elemental projections by using the segmented HAADF-STEM reconstruction as a binary mask during the reconstruction. Since it is reasonable to assume that the total composition in each voxel of the reconstruction equals 1, this constraint is also implemented during the final reconstruction.

Further details regarding the reconstruction algorithm are discussed in the Experimental section.

3. Results and discussion

To demonstrate our approach, we performed the 3D characterization of an octahedral Au/Ag nanorattle with a complex chemical structure. The investigated sample was prepared via the well-known galvanic replacement reaction between Au octahedra@Ag core-shell nanocubes and gold (III) chloride, which is often used to obtain porous and hollow metal nanostructures.[9, 21-24] Due to the presence of cavities and the possible formation of alloys, understanding the 3D structure of such complex particles is far from straightforward based on 2D TEM images. The chemical transformation during a galvanic replacement reaction was recently investigated by 3D XEDS elemental mapping, but only in a qualitative manner.[9, 25] We demonstrate here that quantitative investigation of the Ag distribution is possible in these hollow Au/Ag nanostructures.

HAADF-STEM projections were acquired over a tilt range from -72º to +75º with an increment of 3º. In Figure 3a, the HAADF-STEM image acquired at 0º is presented. Next, XEDS maps were acquired over a tilt range from -70º to +70º with an increment of 10º (more details are provided in the Experimental section). A two window method was used to fit the background radiation and extract the Au and Ag net counts from their respective L lines.[26] As explained above, ratio maps were obtained by using the ζ-factor method.[16] In Figure 3b and Figure 3c, the net counts maps and the ratio maps at 0º are presented. The total net count values for every angle are presented in Figure 4a,b. The total concentrations were calculated for every angle and are presented in Figure 4c,d. The net count values were found to decrease as the tilt angle approached zero, reflecting the position of maximum shadowing from the holder used. At 0º the signal is almost a quarter of the signal that can be collected at ±70º. To

obtain an accurate quantification of the XEDS maps, one needs to be aware of channelling effects that give rise to X-ray signals which are not linearly proportional to the composition. Therefore, the maps should be acquired in off-axis conditions.[27] Also absorption effects will play an important role for samples with a thickness that exceeds the "thin film approximation".[16] Here, as expected in the absence of absorption effects, shadowing has no impact on the concentrations, which show a consistent value over the whole tilt range (Figure 4c,d). The error bars were determined through error propagation as described in the literature.[16, 18, 26] In cases where absorption effects cannot be ignored, it is still possible to obtain a quantitative XEDS reconstruction, but it is necessary to integrate our method with the iterative technique proposed by Burdet et al.[14]

A volume rendering of the HAADF-STEM reconstruction is presented in Figure 5a and its inner structure is illustrated in Figure 5b. Next, thickness maps (Figure 5c) were calculated according to the workflow presented above and were multiplied by the ratio maps to obtain elemental projections (Figure 5d). It's worth mentioning that particular care should be taken in the segmentation step, to ensure that cavities and pores (if present) are excluded from the particle volume. Figure 6 presents an overview of the original maps based on the net counts and the final projections to be used for 3D reconstruction. From Figure 6a,b the effect of shadowing is clear. In Figure 6c,d,e (last three rows) finally, the chemically quantified projections obtained with our method are presented, where shadowing effects have clearly been suppressed. These projections were used to calculate the quantified reconstruction using a Total Variation Minimization (TVM)[28] algorithm based on a Chambolle-Pock solver derived from the work of Sidkey et al.[29] (more details are discussed in the Experimental section).

In Figure 7a,b, 3D visualisations of reconstructions showing the outer and inner structure/composition are presented. Orthoslices through the 3D volume and line profiles are

shown in Figure 7c,d and Figure 7e,f respectively. For an XEDS tomographic series, it can be expected that the projection data is heavily affected by noise. Therefore, also the final reconstruction suffers from a relatively low signal-to-noise ratio which hampers the interpretation of the results. Often filtering of the projections[8, 12, 30] and/or of the final reconstruction is applied.[14] Here, a three-dimensional gaussian filtering of the final reconstructions was performed (Figure 7c). Our results reveal that pure Ag is no longer present and that the inner walls of the cavity consist of a Au/Ag alloy with a variable Ag concentration ranging from 20% to 50%.

Since Au and Ag have a large difference in the atomic number Z, it is rather straightforward in this case to qualitatively distinguish them in the 3D HAADF-STEM reconstruction. For comparison, Figure 8 therefore presents an orthoslice through the chemically quantified reconstruction (Figure 8a) and the corresponding slice through the HAADF-STEM reconstruction (Figure 8b). It can be seen that an excellent correspondence between both approaches is found. These results confirm the validity of our approach. Moreover, the technique that we propose here can also be applied for nanostructures in which more than two elements or elements with similar Z are present. In the latter case, overlapping of peaks in the XEDS spectrum might occur, but the contribution of the different elements can be easily separated by deconvoluting the peaks, in order to obtain the quantified maps.

The Ag distribution, (green in Figure 8a, ~50% w% Ag), accurately matches the distribution of lighter values in the HAADF-STEM reconstruction slice, given by a lower Z-contrast in that area (in this case the values are scaled to arbitrary units), therefore confirming the presence of silver and quantifying its content.

The ability to obtain such information is a clear demonstration of the power of this approach. Further information on the growth of these Au/Ag nanorattles will be presented in a separate paper. It’s worth mentioning that, although we here apply our technique to these structures,

the technique is widely applicable to a broad range of samples. For the interested reader, more discussion is provided in the supporting information.

3. Conclusions

In this paper, we present a synergistic combination of XEDS and HAADF-STEM tomography that enables us to obtain a quantitative 3D reconstruction of the structure and the composition of nanomaterials in a straightforward manner. As an illustration, we applied our method to a complex Au/Ag nanorattle, but the approach is generally applicable to a broad variety of materials. This approach is expected to open doors for the better understanding of complex nanoscale reactions that involve two or more elements as well as composition-dependent properties of nanoscale materials to maximize their efficiency in various applications.

4. Experimental

Synthesis of Octahedral Au/Ag nanorattles with complex composition via galvanic replacement

Octahedral Au/Ag nanorattles were prepared via galvanic replacement reaction between Au@Ag core-shell nanocubes and $HAuCl_4$. Au@Ag core-shell nanocubes were prepared by silver coating on Au nanooctahedra. The synthesis of nanorattles was carried out via the following steps.

Synthesis of Au octahedra

Octahedral Au nanoparticles (NPs) were synthesized by seed-mediated growth.[31] In a typical synthesis, the seed particles were prepared by mixing 2.5 ml of 1 mM $HAuCl_4$ and 7.5 ml of 0.1 M cetyltrimethylammonium bromide (CTAB) aqueous solutions, followed by the rapid addition of 0.6 ml 10 mM freshly prepared, ice-cold $NaBH_4$ solution, under vigorous stirring. After addition of $NaBH_4$, the solution color changes from colorless to brown as a result of the formation of Au seed particles. The as-prepared seed solution was diluted 100 times and then aged at room temperature for 3 h before adding into the growth solution of Au octahedra. Growth solution was prepared by adding 1.2 ml of 0.1 M ascorbic acid to a mixture of 15 ml of 0.05 M $HAuCl_4$ and 3.2 ml of 0.1 M CTAB aqueous solution under stirring. Then, 120 μL of the aged seed solution was added to the growth solution and vigorously mixed for 30 s, and then the reaction mixture was left undisturbed overnight to obtain Au octahedra.

Synthesis of Au@Ag core-shell nanocubes

Au@Ag core-shell nanocubes were prepared by using Au octahedral NPs as seeds. In a typical synthesis, 1 ml of 10 mM $AgNO_3$ and 4 ml of 0.1 M ascorbic acid aqueous solutions were added to 10 ml of as prepared Au octahedral NPs solution under stirring. The solution was kept in an oven at 60 °C overnight to complete the growth and the solution color turns into yellow, indicating the formation of Au@Ag core-shell NCs.

Galvanic replacement reaction between Au@Ag core-shell nanocubes and $HAuCl_4$

The as-prepared nanocubes were purified by centrifugation at 8000 rpm for 20 min and then re-dispersed in same volume of 0.1 M CTAB for galvanic replacement. Typically, 3 ml of 0.5 mM $HAuCl_4$ aqueous solution were added to a mixture of 5 ml of the purified Au@Ag nanocubes and 0.2 ml of 0.1 M ascorbic acid, using a syringe pump at a rate of 50 μL/min under continuous stirring. The obtained particles were purified by centrifugation at 8000 rpm for 20 min and then re-dispersed in water.

Data acquisition

The tomographic series were acquired using an aberration corrected cubed FEI Titan 60-300 electron microscope operated at 200 kV, equipped with a Super-X detector. HAADF-STEM projections were acquired over a tilt range from -72º to +75º with an increment of 3º. XEDS maps were acquired over a tilt range from -70º to +70º with an increment of 10º. The acquisition time for each map equals 3 minutes and a screen current of approximately 250 pA, was applied.

The data was binned to a canvas of 52*52 pixels to improve the number of counts per pixel and a two window method[26] was used to fit the background radiation and extract the Au and Ag net counts from their relative L lines. Quantified ratio maps were obtained by using the ζ-factor method[16] and ζ-factors obtained as described in previous work.[submitted] The ζ-

factors values for Au and Ag, were respectively: ζ_{Au} = 1177 ± 93 kg/m^2 and ζ_{Ag} = 492 ± 46 kg/m^2.

In order to combine the XEDS and STEM data while preserving details of the morphology and performing the reconstruction on a larger voxel grid, the ratio maps were scaled up to the size of the forward projections (268x268 pixels), using a *nearest neighbor* interpolation method, which avoids blurring and preserves the original distribution and 'look' of the quantified pixels (see Figure 5d and Figure 6).

Data processing and reconstruction

The tomographic tilt series were registered through cross-correlation routines implemented in Matlab.[20] Once aligned, the series were reconstructed using the ASTRA[32, 33] and SPOT toolboxes.[34, 35] The reconstruction algorithm was implemented by generating the projection matrix and using a Chambolle-Pock[29, 36] solver to perform a Total Variation Minimization[28] (TVM) reconstruction.

The HAADF-STEM reconstruction was segmented according to its histogram (selecting the gray value corresponding to the first minimum of the histogram), determining the shape of the particle, and forward projected (with the ASTRA toolbox) along the directions used to acquire the XEDS maps. In this manner the particle thickness relative to the ratio maps was measured. In the case of the XEDS reconstruction, the Chambolle-Pock solver was modified to include a constraining mask, implementing prior-knowledge on the shape of the particle (obtained from the HAADF-STEM reconstruction) and on the concentrations in the final reconstruction (e.g. $C_{Au} + C_{Ag} = 1$ in every voxel).

Acknowledgement

The authors acknowledge financial support from European Research Council (ERC Starting Grant # 335078-COLOURATOMS, ERC Advanced Grant # 291667 HierarSACol and ERC Advanced Grant 267867 - PLASMAQUO), the European Union under the FP7 (Integrated Infrastructure Initiative N. 262348 European Soft Matter Infrastructure, ESMI and N. 312483 ESTEEM2).

Table of Contents

A new method to quantify XEDS data in 3D is presented. The synergistic combination of XEDS quantification and HAADF-STEM tomography, enables to overcome the "shadowing" problem and obtain an accurate chemically quantified 3D reconstruction of the structure investigated. As a proof of principle, the technique is used to determine the elements distribution in a complex Au/Ag nanorattle.

Keyword (see list)

D. Zanaga, T. Altantzis, L. Polavarapu, L. M. Liz-Marzán, B. Freitag, S. Bals*

Quantitative XEDS tomography of complex hetero-nanostructures

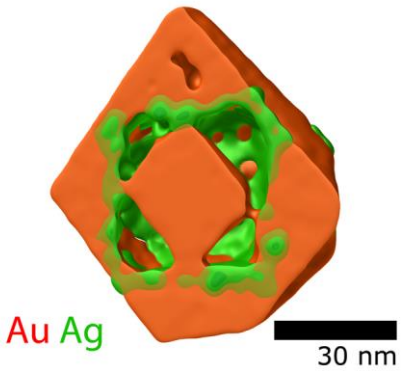

Figures

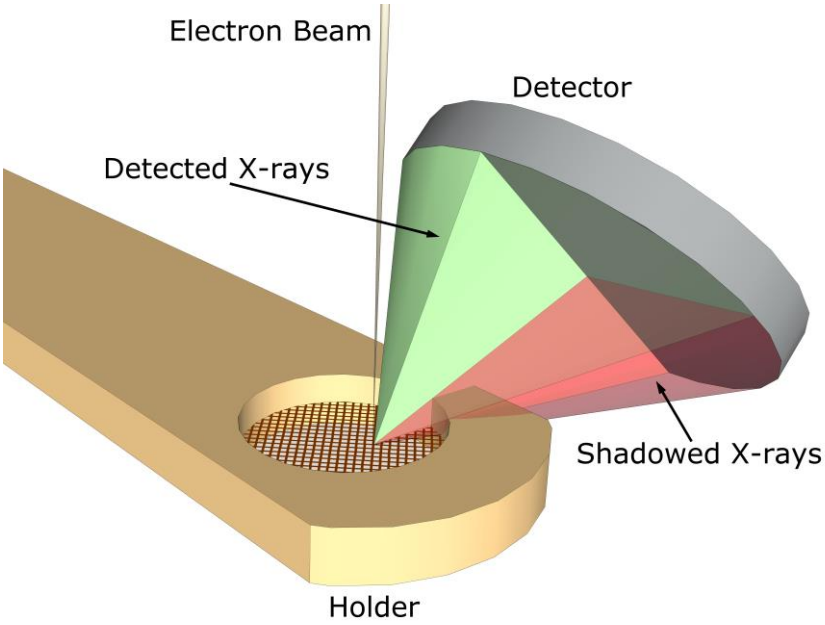

Figure 1: The figure schematically shows how detection of X-rays is hampered by the holder. The detectable X-rays emitted from the sample are indicated by the green cone, while those blocked by the holder are indicated by the red cone. Only one of the four Super-X detectors is depicted, but the scheme holds generally for all detectors. Upon tilting the sample, the effect of shadowing changes as a function of the tilt angle.

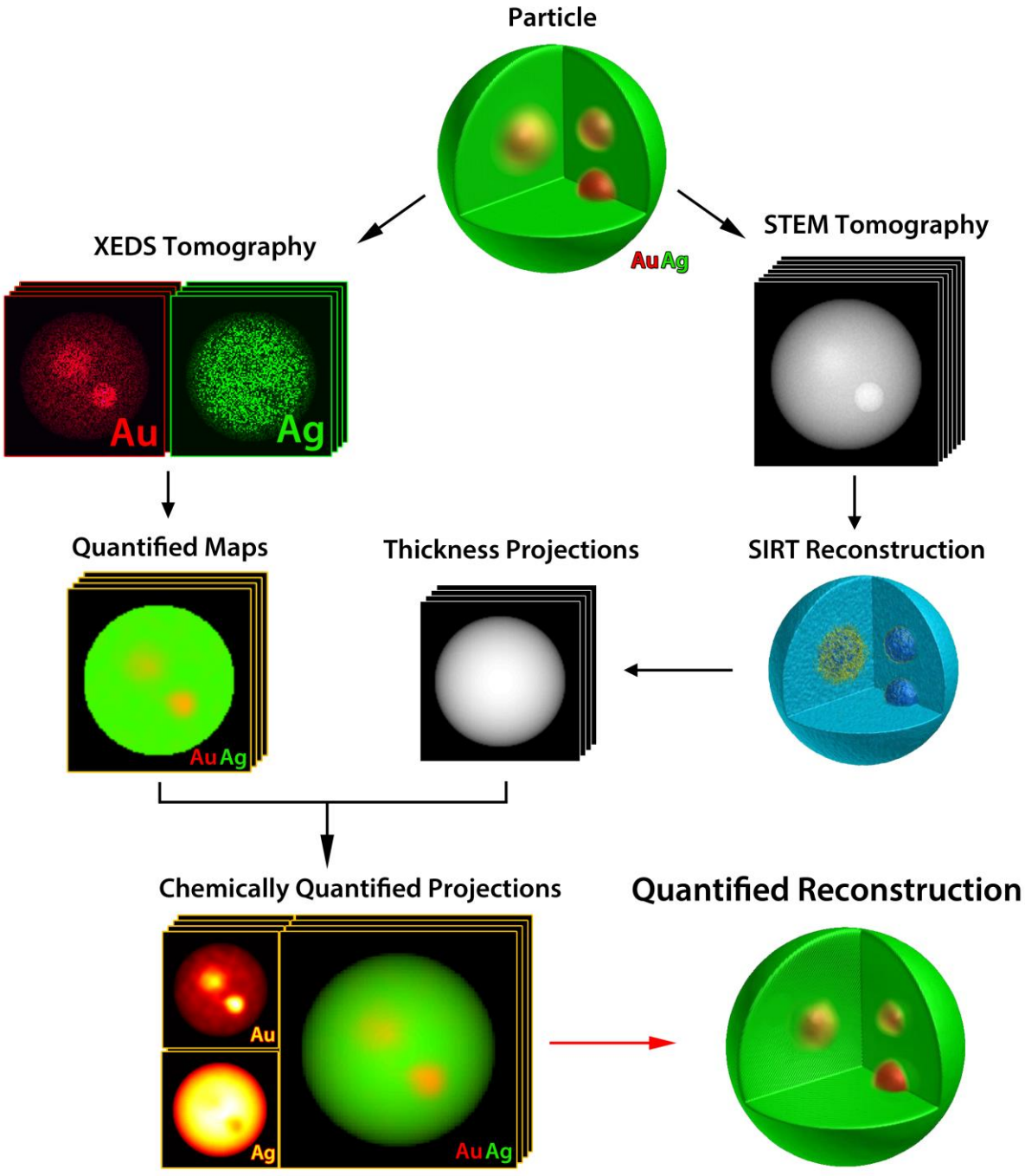

Figure 2: The figure schematically shows the principal steps of the technique proposed on a simulated particle of Au and Ag.

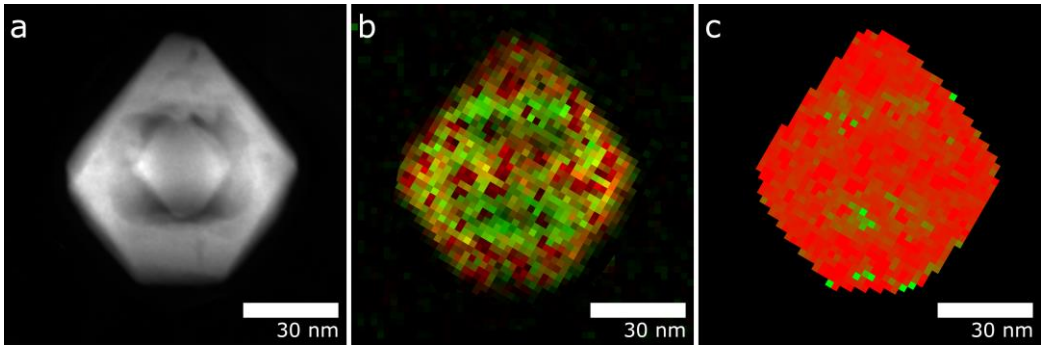

Figure 3: (a) HAADF-STEM projection at 0°. (b) XEDS net counts maps for Au (red) and Ag (green) after background subtraction. (c) Ratio map obtained with the ζ-factor method.

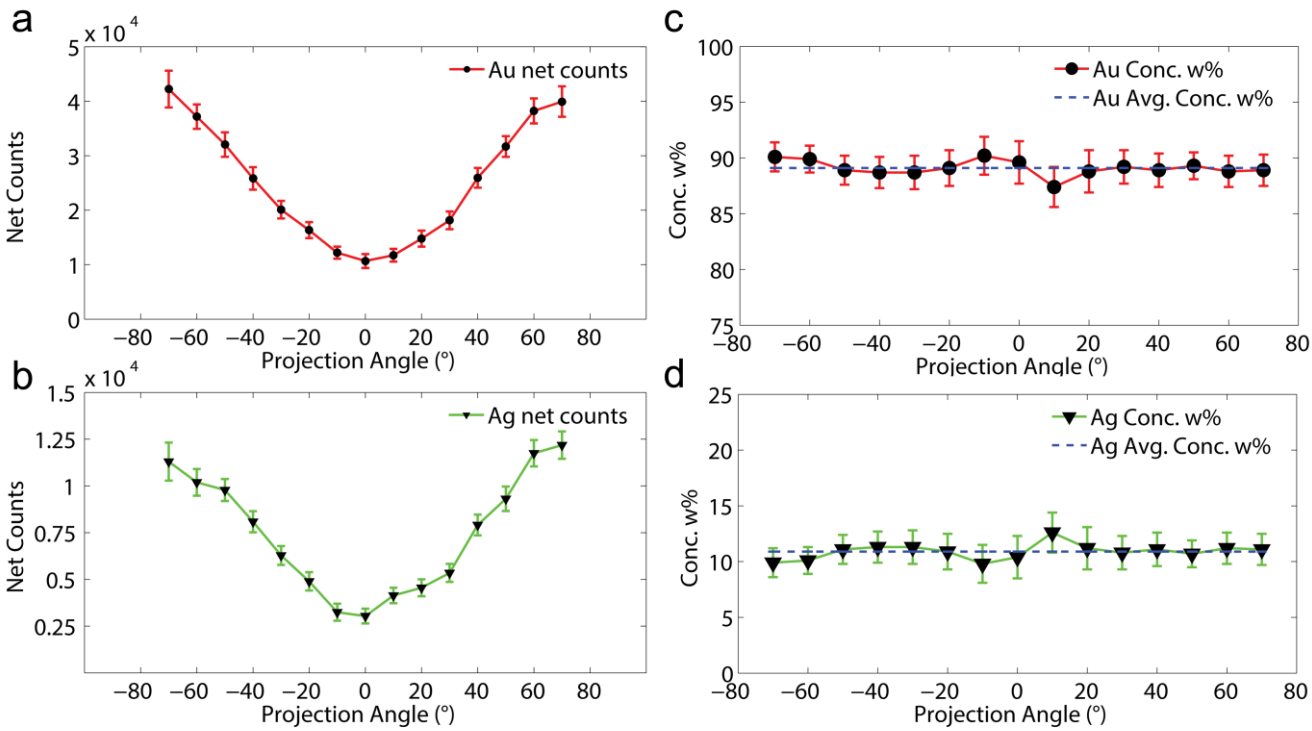

Figure 4: (a,b) Au and Ag total net counts for every dataset acquired from -70° to +70°. (c,d) Au and Ag concentration as a function of the acquisition angle, calculated with the ζ-factor method. Single values are consistent with the average value calculated (dashed blue line) as expected in the presence of negligible absorption effects.

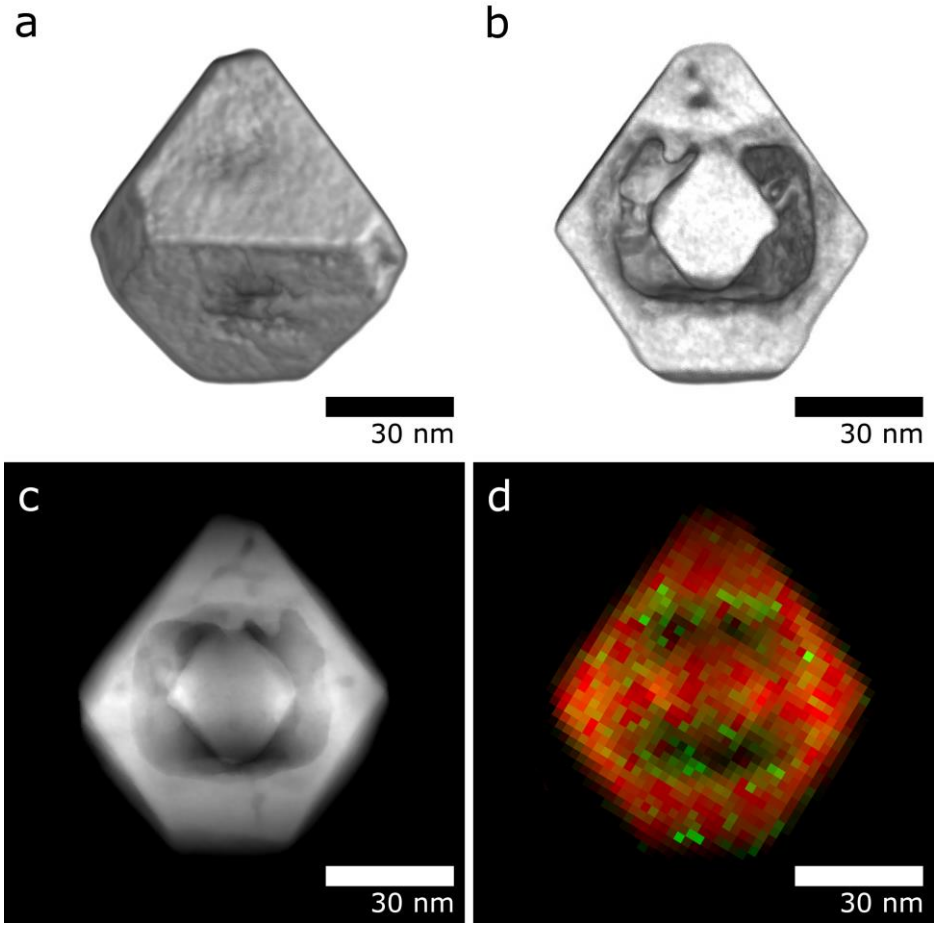

Figure 5: (a) Volume rendering of the HAADF-STEM reconstruction. (b) Inner structure of the same reconstruction. (c) Forward projections of the segmented SIRT reconstruction, corresponding to the thickness of the particle expressed in voxel units. (d) Chemically quantified elemental projection obtained by multiplying the XEDS quantified map of Figure 3c and the forward projection of Figure 5c.

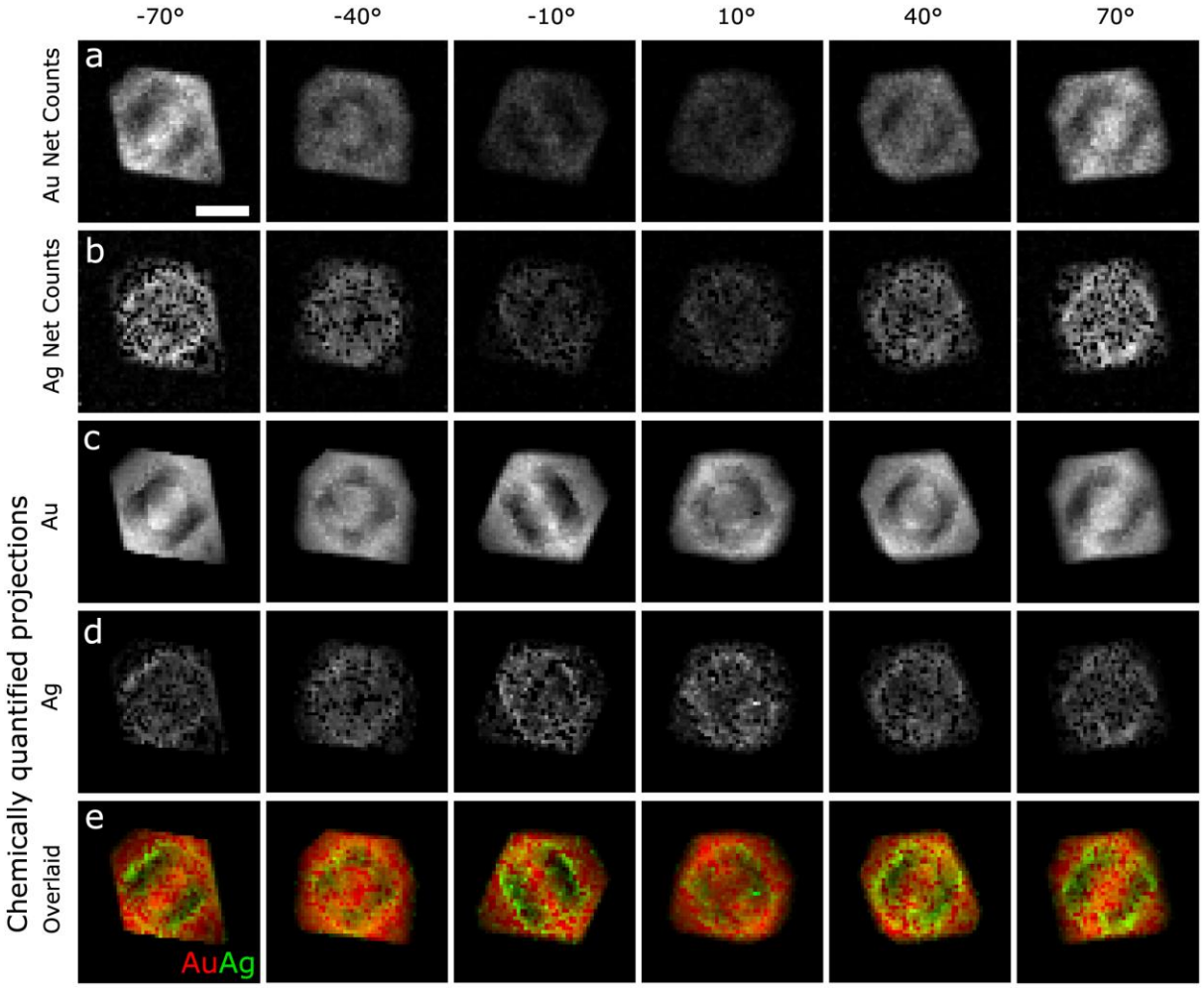

Figure 6: (a,b) Au and Ag net counts maps. The decrease of signal in projections close to 0° is due to shadowing effects. (c,d) Au and Ag chemically quantified projections obtained with the method presented in this paper. The signal now scales linearly with thickness and concentration of the elements, satisfying the projection requirement. (e) Au and Ag chemically quantified projections overlaid with different colors. The scale bar in Figure 6a (first tile of the row) is 30 nm. To enable a correct visualization of the images, the intensity range is normalized between the maximum and the minimum value of each row of images.

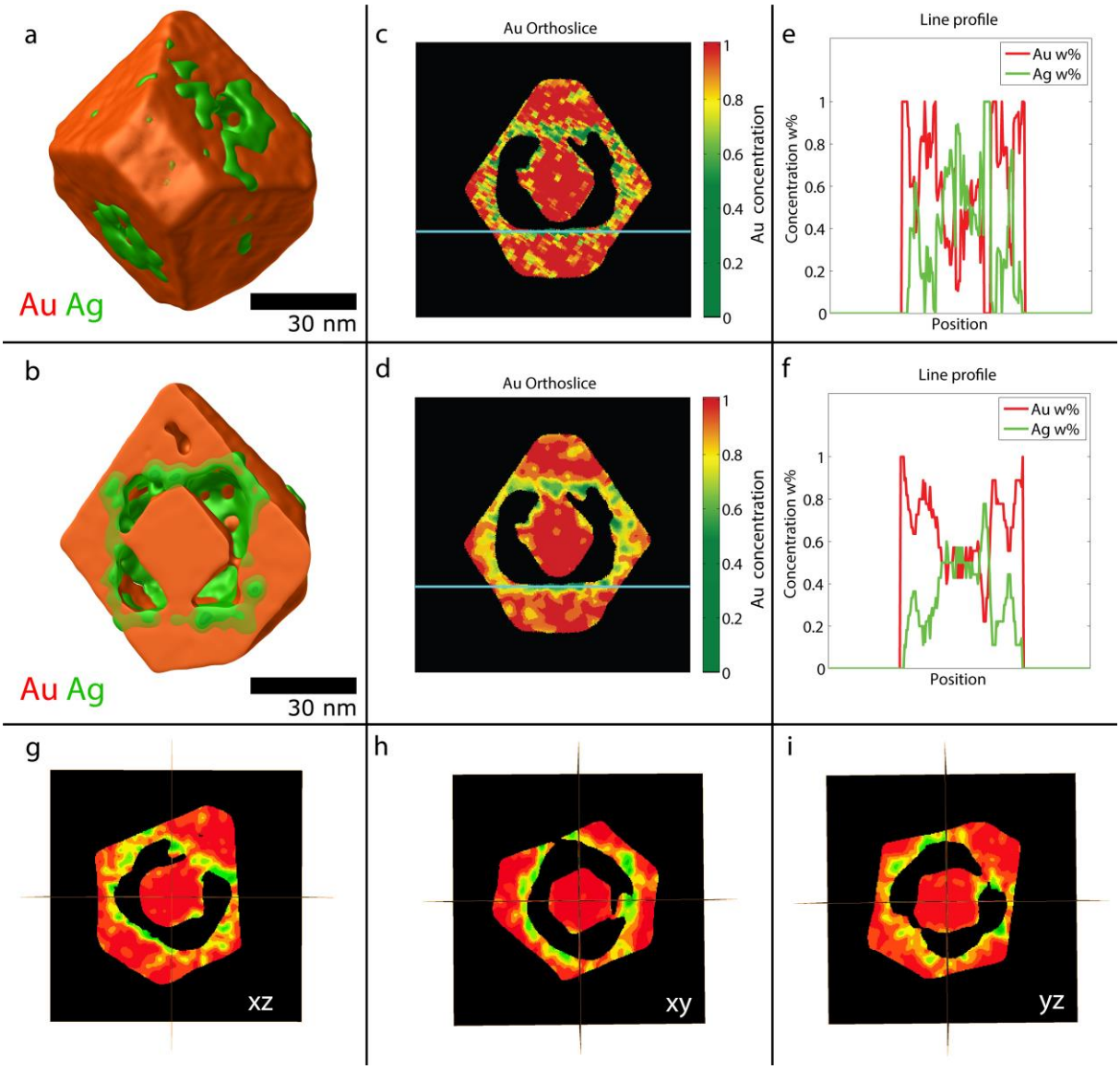

Figure 7: (a) Volume rendering of the Au (red) and Ag (green) quantified reconstructions obtained with the presented method. (b) Inner composition of the same reconstructions. (c) Orthoslice through the Au reconstruction showing the concentration in every voxel, through a red-green color-map. (d) Similar to Figure 7c but applying a 3D Gaussian filter. In (c,d) pixel values not belonging to the particle are displayed in black. (e) Line profile, showing weight concentration values of the quantified reconstructions. The voxels along which the profile is extracted are indicated by the blue line in Figure 7c. (f) Line profile relative to Figure 7d.

(g,h,i) Orthogonal orthoslices of the reconstructed volume, respectevely of planes xz, xy and yz. The colorbar is the same used in Figure 7c,d.

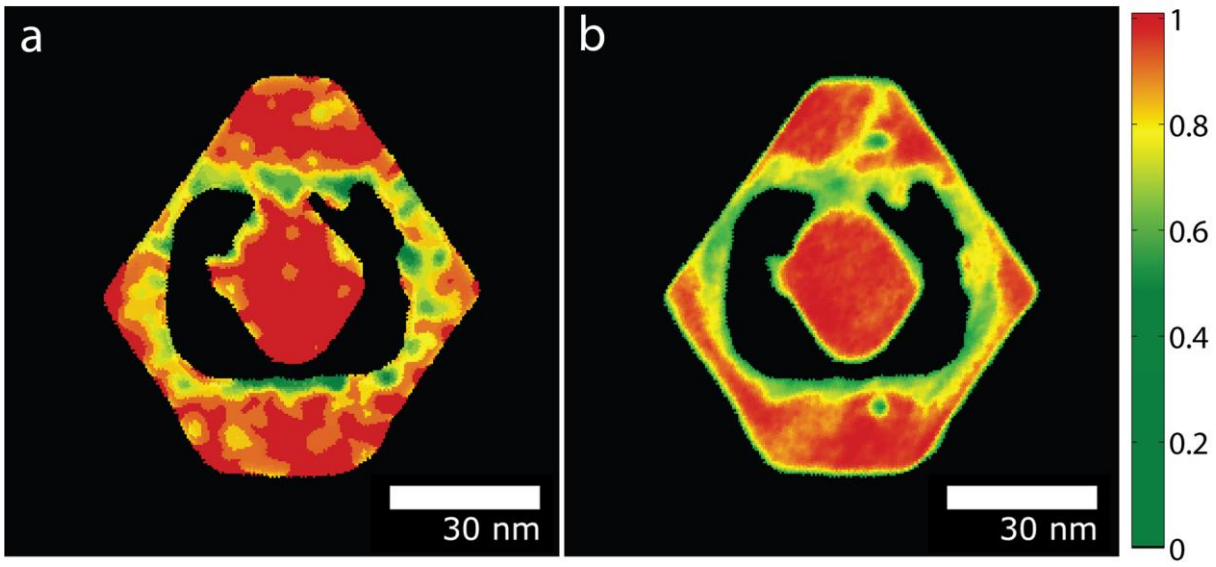

Figure 8: (a) XEDS 3D quantified reconstruction, after filtering with a 3D Gaussian filter to enable an easier interpretation, the color bar on the right reflects the concentration values of Au (b) Slice from the HAADF-STEM 3D reconstruction, arbitrarily scaled to match the values range of the XEDS reconstruction and enable the comparison of the elements distribution.

References

[1] P. Midgley, M. Weyland, Ultramicroscopy **2003**, 96, 413.
[2] I. Arslan, T. Yates, N. Browning, P. Midgley, Science **2005**, 309, 2195.
[3] S. Pennycook, Ultramicroscopy **1989**, 30, 58.
[4] L. M. Liz-Marzán, Langmuir **2006**, 22, 32.
[5] P. Schlossmacher, D. Klenov, B. Freitag, H. Von Harrach, Microscopy today **2010**, 18, 14.
[6] S. Kawai, I. Onishi, T. Ishikawa, K. Yagi, T. Iwama, K. Miyatake, Y. Iwasawa, M. Matsushita, T. Kaneyama, Y. Kondo, Microscopy and Microanalysis **2014**, 20, 1150.
[7] A. Genç, H. Cheng, J. Winterstein, L. Pullan, B. Freitag, Microscopy and Analysis **2012**, 116, 23.
[8] A. Genc, L. Kovarik, M. Gu, H. Cheng, P. Plachinda, L. Pullan, B. Freitag, C. Wang, Ultramicroscopy **2013**, 131, 24.
[9] B. Goris, L. Polavarapu, S. Bals, G. Van Tendeloo, L. M. Liz-Marzán, Nano letters **2014**, 14, 3220.
[10] N. Liakakos, C. Gatel, T. Blon, T. Altantzis, S. Lentijo-Mozo, C. c. Garcia-Marcelot, L.-M. Lacroix, M. Respaud, S. Bals, G. Van Tendeloo, Nano letters **2014**, 14, 2747.
[11] B. Goris, B. Freitag, D. Zanaga, E. Bladt, T. Altantzis, J. Ringnalda, S. Bals, Microscopy and Microanalysis **2014**, 20, 766.
[12] T. J. Slater, A. Janssen, P. H. Camargo, M. G. Burke, N. J. Zaluzec, S. J. Haigh, Ultramicroscopy **2015**.
[13] T. Slater, P. Camargo, M. Burke, N. Zaluzec, S. Haigh, "Understanding the limitations of the Super-X energy dispersive x-ray spectrometer as a function of specimen tilt angle for tomographic data acquisition in the S/TEM", presented at *Journal of Physics: Conference Series*, **2014.**
[14] P. Burdet, Z. Saghi, A. N. Filippin, A. Borrás, P. A. Midgley, Ultramicroscopy **2015**.
[15] G. Haberfehlner, A. Orthacker, M. Albu, J. Li, G. Kothleitner, Nanoscale **2014**, 6, 14563.
[16] M. Watanabe, D. Williams, Journal of microscopy **2006**, 221, 89.
[17] G. Cliff, G. Lorimer, Journal of Microscopy **1975**, 103, 203.
[18] D. Zanaga, T. Altantzis, J. Sanctorum, B. Freitag, S. Bals, *Submitted* **2016**.
[19] P. Gilbert, Journal of theoretical biology **1972**, 36, 105.
[20] M. Guizar-Sicairos, S. T. Thurman, J. R. Fienup, Optics letters **2008**, 33, 156.
[21] M. H. Oh, T. Yu, S.-H. Yu, B. Lim, K.-T. Ko, M.-G. Willinger, D.-H. Seo, B. H. Kim, M. G. Cho, J.-H. Park, Science **2013**, 340, 964.
[22] J. Chen, B. Wiley, J. McLellan, Y. Xiong, Z.-Y. Li, Y. Xia, Nano letters **2005**, 5, 2058.
[23] Y. Sun, Y. Xia, Nano Letters **2003**, 3, 1569.
[24] L. Polavarapu, L. M. Liz-Marzán, Nanoscale **2013**, 5, 4355.
[25] T. J. Slater, A. Macedo, S. L. Schroeder, M. G. Burke, P. O'Brien, P. H. Camargo, S. J. Haigh, Nano letters **2014**, 14, 1921.
[26] D. B. Williams, C. B. Carter, *The transmission electron microscope*, Springer, **1996**.
[27] G. Kothleitner, M. Neish, N. Lugg, S. Findlay, W. Grogger, F. Hofer, L. Allen, Physical Review Letters **2014**, 112, 085501.
[28] B. Goris, W. Van den Broek, K. J. Batenburg, H. H. Mezerji, S. Bals, Ultramicroscopy **2012**, 113, 120.
[29] E. Y. Sidky, J. H. Jørgensen, X. Pan, Physics in medicine and biology **2012**, 57, 3065.
[30] K. Lepinay, F. Lorut, R. Pantel, T. Epicier, Micron **2013**, 47, 43.
[31] A. Jaiswal, L. Tian, S. Tadepalli, K. k. Liu, M. Fei, M. E. Farrell, P. M. Pellegrino, S. Singamaneni, Small **2014**, 10, 4287.
[32] W. J. Palenstijn, K. J. Batenburg, J. Sijbers, Journal of structural biology **2011**, 176, 250.
[33] W. van Aarle, W. J. Palenstijn, J. De Beenhouwer, T. Altantzis, S. Bals, K. J. Batenburg, J. Sijbers, Ultramicroscopy **2015**, 157, 35.

[34] F. Bleichrodt, T. Van Leeuwen, W. J. Palenstijn, W. Van Aarle, J. Sijbers, K. J. Batenburg, Numerical Algorithms **2015**.
[35] E. van den Berg, M. Friedlander, **2009**, http://www.cs.ubc.ca/labs/scl/spot, accessed: June, 2015.
[36] A. Chambolle, T. Pock, Journal of Mathematical Imaging and Vision **2011**, 40, 120.